Journal of Materials Chemistry

Cite this: DOI: 10.1039/c2jm30448a

www.rsc.org/materials

PAPER

Sponge-like porous carbon/tin composite anode materials for lithium ion batteries

Yunhua Xu, Juchen Guo and Chunsheng Wang*

Received 21st January 2012, Accepted 8th March 2012
DOI: 10.1039/c2jm30448a

A novel sponge-like porous C/Sn composite is synthesized by dispersing SnO_2 nanoparticles into a soft-template polymer matrix followed by carbonization. The mesoporous C/Sn anodes can deliver a capacity as high as 1300 mAh g^{-1} after 450 charge/discharge cycles, and provide a capacity of 180 mAh g^{-1} even at 4000 mA g^{-1} charge/discharge current density. An extra reversible capacity over the theoretical value of the porous C/Sn anode is observed, which is attributed to the reversible formation/decomposition of the gel-like polymers formed on the mesoporous C/Sn composite due to the catalytic effect of the Sn nanoparticles. The high capacity, long cycle life, high power, ~100% Coulombic efficiency, and inexpensive production method make the sponge-like porous C/Sn composite an attractive anode material in Li-ion batteries for electric vehicles and renewable energy storage.

Introduction

Development of rechargeable batteries with high capacity, high rate capability, and long cycling life is the key to the success of electric vehicles (EVs) and the use of renewable energies, such as wind and solar energies. Lithium ion batteries, the most popular power sources on the market for portable electronic devices, can be used for EVs if the energy density can be enhanced.[1] In the last decade, extensive efforts have been made to increase the capacity of anodes by replacing the currently used graphite with Si or Sn.[2–5] Although Si has a higher gravimetric capacity (3572 mAh g^{-1}) than that of Sn (992 mAh g^{-1}), their volumetric capacities are similar (8322 mAh cm^{-3} for Si and 7254 mAh cm^{-3} for Sn), and both are considerably larger than that of graphite (818 mAh cm^{-3}). The volumetric energy density is the most relevant metric for most Li-ion battery applications.[6] However, the practical application of Sn anodes is hampered by the poor cycling stability due to a large volume change of 260% as well as aggregation during the lithiation/delithiation processes.[7–15] The strain-induced pulverization would lead to a loss in contact with the current collector, resulting in a fast capacity fading.

The most successful method for improving the cycling stability is to form a C/Sn nanocomposite.[13–15] Electro-spinning has been used to synthesize C/Sn composites by dispersing Sn nanoparticles in porous multichannel carbon microtubes[10] or bamboo-like hollow carbon nanofibers.[11] The porous C/Sn composite materials have two-fold advantages: (1) the porous structure of the C/Sn composites provides additional space to accommodate the volume variation, reducing the tin particle pulverization; (2) the porous carbon matrix can avoid the oxidation and aggregation of Sn nanoparticles and provides a continuous electron pathway. However, the electro-spinning synthesis approach still faces challenges to control the morphology and component ratio of C/Sn. Therefore, a simple route for the synthesis of porous C/Sn composite anode materials is highly desired, especially for transforming the research efforts into commercial products.

In this paper, a novel sponge-like mesoporous C/Sn composite was prepared using a soft-template method[16–18] by carbonizing phase-separated polymer/SnO_2 nanoparticle composite precursor. SnO_2 nanoparticles were reduced to Sn nanoparticles under presence of carbon during the carbonization process. Resorcinol-formaldehyde (RF) was used as the carbon source, and a triblock copolymer of poly(ethylene oxide)-*b*-poly(propylene oxide)-*b*-poly(ethylene oxide) (EO_{106}-PO_{70}-EO_{106}, Pluronic F127) was used as the sacrificial template to form pores in the carbon. The interaction between these two polymers promoted a self-assembled nanostructure through phase-separation. The template block copolymer decomposed in the subsequent carbonization to form pores, and the RF polymer framework was carbonized as the carbon walls. The resulting porous carbon exhibited a large pore volume and thin carbon walls, making it like a carbon sponge. Tin nanoparticles were well dispersed in this unique porous structure that can accommodate the large volume change during charge/discharge cycling. The resiliency and conductivity of the carbon walls could provide a mechanical support to alleviate tin particle pulverization and ensure good electric contact.[13,14,19,20] The aggregation of tin particles could also be prevented by the carbon sponge.[9,12] With these features, a high specific capacity and a long cycling life are expected from this porous C/Sn nanoparticle composite anode material for lithium ion batteries.

Department of Chemical and Biomolecular Engineering, University of Maryland, College Park, MD 20742, USA. E-mail: cswang@umd.edu

Experimental

Synthesis of porous carbon/tin nanoparticle composite

The synthesis of the porous C/Sn composite materials consisted of three steps: preparation of polymer solution, SnO_2 nanoparticle dispersion, and carbonization. All materials were purchased from Sigma-Aldrich and were used without further purification. The polymer solution was prepared by dissolving 0.33 g resorcinol (R), 0.22 g triblock copolymer (Pluronic F127) and 1 ml 1% NaOH aqueous solution in 5 ml *N*,*N*-dimethylformamide (DMF), where the triblock copolymer and the NaOH functioned as the soft-template and catalyst, respectively. When the solution was clear, 0.4 g 37% formaldehyde (F) aqueous solution was added. After 30 min vigorous stirring, the solution was stirred for another 30 min at 80 °C to promote the polymerization reaction between resorcinol and formaldehyde. In the meantime, 0.5 g SnO_2 nanoparticles (<100 nm) were dispersed into 30 ml DMF by ultrasonication. Then the obtained solution was added into the dispersion and underwent ultrasonic treatment. The mixture was dried while stirring at 100 °C overnight and was further cured in an oven at 100 °C for 24 h. Finally, the polymer/SnO_2 composite was carbonized with a heating rate of 2 °C min^{-1} in flowing argon at 400 °C for 3 h and then at 700 °C for an additional 3 h. For comparison, porous carbon without Sn was synthesized using the same procedure described above.

Material characterizations

Scanning electron microscopy (SEM) and transmission electron microscopy (TEM) images were taken by a Hitachi SU-70 analytical ultra-high resolution SEM (Japan) and a JEOL (Japan) 2100F field emission TEM, respectively. The X-ray diffraction (XRD) pattern was recorded by a Bruker Smart1000 (Bruker AXS Inc., USA) using Cu-Kα radiation. Thermogravimetric analysis (TGA) was carried out using a thermogravimetric analyzer (TA Instruments, USA) with a heating rate of 10 °C min^{-1} in air. The BET specific surface area and pore size and volume were analyzed using N_2 absorption on a TriStar 3020 (Micromeritics Instrument Corp., USA).

Electrochemical measurements

The porous C/Sn composite was mixed with carbon black and sodium carboxymethyl cellulose (CMC) binder to form a slurry at the weight ratio of 70 : 15 : 15. The electrode was prepared by casting the slurry onto copper foil using a doctor blade and drying in a vacuum oven at 100 °C overnight. Coin cells were assembled with lithium foil as the counter electrode, 1 M $LiPF_6$ in a mixture of ethylene carbonate/diethyl carbonate (EC–DEC, 1 : 1 by volume) as the electrolyte, and Celgard®3501 (Celgard, LLC Corp., USA) as the separator. Cells with pure porous carbon electrodes were also fabricated using the same procedure. The electrochemical performance was tested using an Arbin battery test station (BT2000, Arbin Instruments, USA). The capacity was calculated on the basis of the total mass of the porous C/Sn composite. The cyclic voltammogram scanned at 0.2 mV s^{-1} between 0–3 V was recorded using a Solartron 1260/1287 Electrochemical Interface (Solartron Metrology, UK).

Results and discussion

Structure of the porous C/Sn composite

Fig. 1a shows the SEM image of the porous C/Sn composite. It is clearly seen that tin nanoparticles with a particle size of around 100 nm are uniformly embedded in a sponge-like porous carbon matrix. Pores with a diameter of around 10 nm are separated by very thin carbon walls. The unique sponge-like carbon matrix will provide a large void space and mechanical support to release the strain induced by the alloying/dealloying of tin, thus preventing the pulverization of tin particles.

The Sn particle size and distribution in the carbon sponge were also investigated using TEM, as shown in Fig. 1b and c. Sn nanoparticles with an average particle diameter of about 100 nm were uniformly dispersed in the porous carbon matrix, which is consistent with SEM results. The particle size is similar to that of

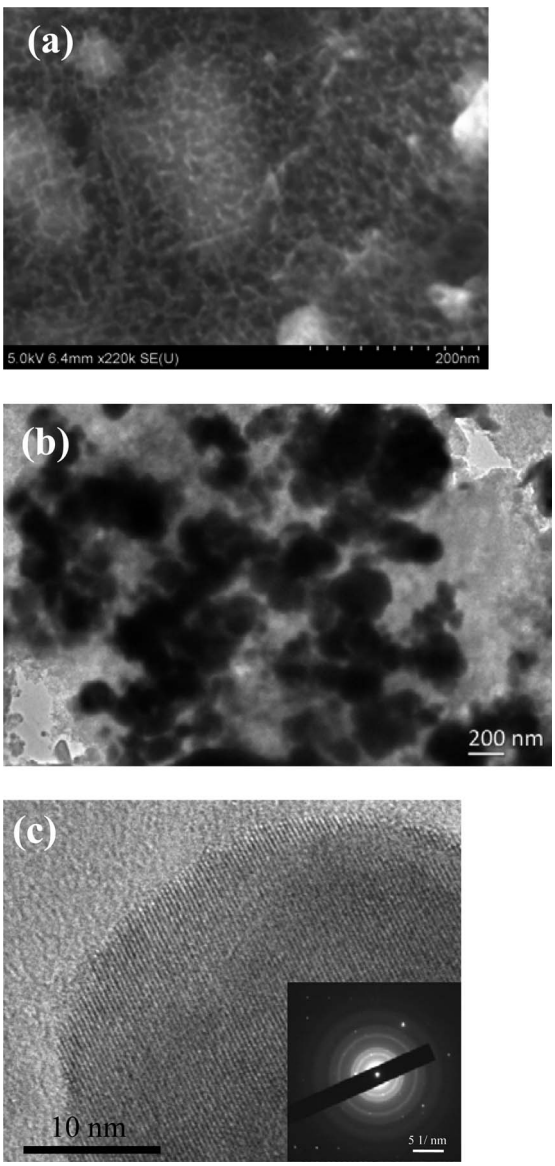

Fig. 1 (a) SEM, (b) TEM, and (c) HRTEM images of the porous C/Sn composite. Inset: SAED pattern of tin nanoparticles.

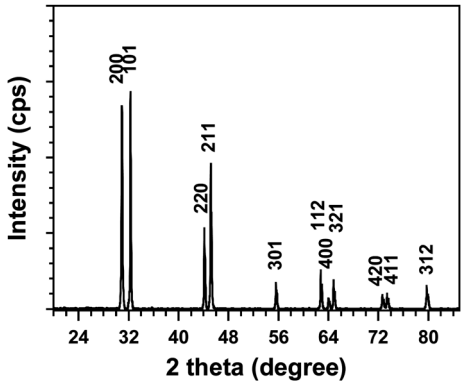

Fig. 2 XRD pattern of the porous C/Sn composite.

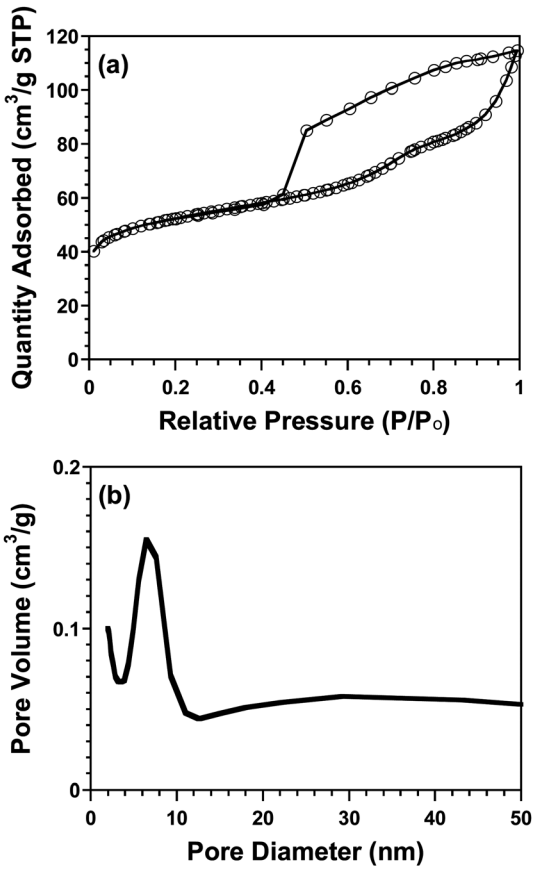

Fig. 3 (a) N_2 adsorption/desorption isotherm and (b) pore-size distribution curve of the porous C/Sn composite.

the SnO_2 nanoparticles which were used as the tin source, demonstrating that the Sn nanoparticles were well dispersed and confined in the carbon matrix, and no aggregation occurred even when Sn became liquid during carbonization at a temperature higher than the melting point of tin metal. These results suggested that the sponge-like carbon matrix may prevent the aggregation of tin particles during prolonged cycling, improving the cycling stability. High-resolution transmission electron microscopy (HRTEM) and selected area electron diffraction (SAED) images (Fig. 1c and inset) revealed that the Sn nanoparticles have a crystalline structure, which was also confirmed

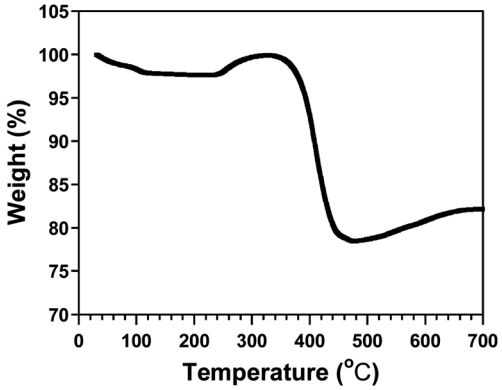

Fig. 4 Thermogravimetric (TGA) curve of porous C/Sn composite in air.

by the X-ray diffraction (XRD) pattern (Fig. 2). All the peaks in Fig. 2 could be indexed to crystalline tin (JCPDS card no. 86-2264). No peaks attributed to SnO_2 were detected, indicating that the SnO_2 particles were completely converted to crystalline tin.

The porous structure of the C/Sn composite was characterized by N_2 adsorption measurement. Fig. 3 depicts the adsorption isotherm and the pore size distribution analyzed by the Barrett–Joyner–Halenda (BJH) method. The Brunauer–Emmett–Teller (BET) specific surface area of the porous C/Sn composite is 180 $m^2\ g^{-1}$ and the pore volume is 0.16 $cm^3\ g^{-1}$. The BJH average pore diameter is 7 nm (Fig. 3b), which is in accordance with previous reports.[16,17] The large specific surface area and pore volume would be beneficial to alleviating strain, accommodate volume changes and improve the kinetics.

Composition and stability of porous C/Sn composite

The composition and thermal/chemical stability of the porous C/Sn composite were measured in air using TGA analysis (shown in Fig. 4). The small weight loss below 100 °C in Fig. 4 was attributed to water evaporation. Almost no weight loss between 100 °C to 220 °C can be observed, demonstrating that both carbon and Sn in the porous C/Sn composite are thermally and chemically stable in air up to 220 °C, *i.e.* no Sn oxidation reaction and carbon decomposition occurred in air at 220 °C. Therefore, the sponge-like mesoporous carbon/Sn composite prepared using the soft-template method can be stored for a long-time without performance decline.[13,21] The weight gain from 220 °C to 300 °C is attributed to the oxidation of metallic tin ($Sn + O_2 \rightarrow SnO_2$), while the subsequent weight loss from 300 °C to 480 °C is mainly due to carbon decomposition ($C + O_2 \rightarrow CO_2$ (gas)).[13] The content of metallic tin in the composite was determined to be 66% using the following eqn (1):

$$S(\mathrm{wt\%}) = 100 \times \frac{\text{molecular weight of Sn}}{\text{molecular weight of } SnO_2} \times \frac{\text{final weight of } SnO_2}{\text{initial weight of C/Sn composite}} \quad (1)$$

Electrochemical performance of porous C/Sn composite

The electrochemical behaviors of the porous C/Sn composite electrodes were investigated in coin-style half cells using lithium

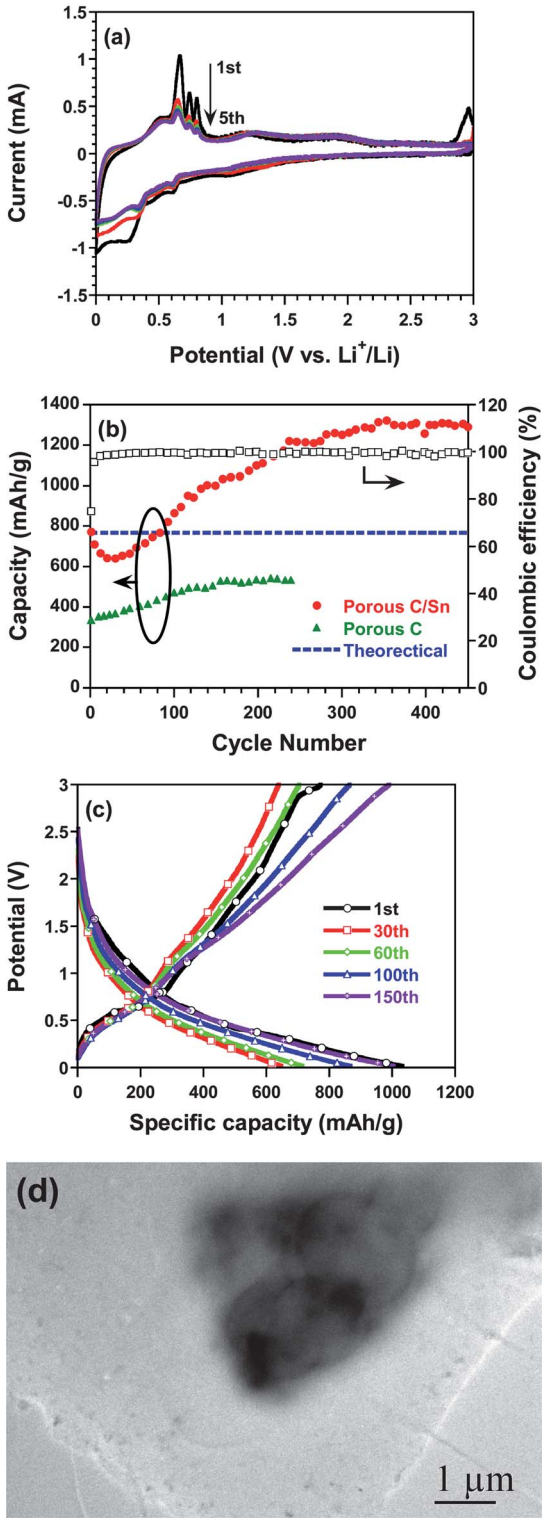

Fig. 5 (a) Cyclic voltammograms of the initial 5 cycles of the porous C/Sn. (b) Cycling performance of the porous C/Sn composite (circles), porous carbon without tin nanoparticles (triangles) and the theoretical capacity of the porous C/Sn composite based on the capacity of pure porous carbon and the theoretical capacity of metallic tin (dashed line). (c) Charge/discharge profiles at the 1st, 30th, 100th, and 150th cycles. (d) TEM image of porous C/Sn anode charged to 1 V.

as the counter electrode. Fig. 5a shows the cyclic voltammograms of the initial 5 cycles. Two reduction peaks at 0.33 V and 0.6 V, are assigned to the lithiation reaction between tin and lithium to form the Li_xSn alloy.[13,15,22] The corresponding oxidation peaks between 0.4 V and 0.8 V were assigned to the delithiation reaction of the Li_xSn alloy.[13,15,22] The peak currents due to the lithiation/delithiation of Sn were stabilized after an initial small decline in the first three charge/discharge cycles. Two irreversible peaks at 1.05 V and 1.55 V, responsible for the catalytic decomposition of the electrolyte on tin, were not observed in the first lithiation. Therefore, it indicated that the tin nano-particles were completely encapsulated in the carbon matrix.[15] The reason for the abnormal peak near 3 V, which occurred only in the first oxidation scan and was also reported on the C/Sn composite by other researchers,[23] was still not fully understood.

Fig. 5b illustrated the cycling stability of the porous C/Sn composite at a current density of 200 mA g^{-1} between 0.02–3 V. For comparison, the cycling behavior of porous carbon without tin nanoparticles was also evaluated under the same conditions. The theoretical capacity of the porous C/Sn composite (Sn : C = 66 : 34 by weight), based on the theoretical capacity of metallic tin (992 mAh g^{-1}) and the actual capacity of pure porous carbon (335 mAh g^{-1}) in the first-cycle, was also shown in Fig. 5b. The capacity of the porous C/Sn composite in the first delithiation was 769 mAh g^{-1}, which was close to the theoretical capacity of the Sn and carbon composite (770 mAh g^{-1}). The specific capacity of the C/Sn composite gradually decreased to 620 mAh g^{-1} during the initial 30 charge/discharge cycles, and then began to increase and become stabilized at 1300 mAh g^{-1} after 300 cycles. Since the capacity of pure porous carbon continuously increased with the charge/discharge cycles, the initial capacity decline of the porous C/Sn anodes should be attributed to a slight degeneration of the nano-Sn particles. The stabilized capacity of 1300 mAh g^{-1} after 300 cycles is much higher than that of the current commercially used graphite and even higher than the theoretical capacity (770 mAh g^{-1}) of the composite. A similar capacity increasing behavior during charge/discharge cycles has also been reported on porous carbon,[24] SnO_2/graphene nanocomposites,[25] and Si/C nanocomposite anode materials[26] in lithium ion batteries. The mechanism behind it is still not clear. Extra capacity over the theoretical capacity was also found in metal oxide anodes (such as CoO,[27,28] CuO,[29] and SnO_2[23]), where the extra capacity was attributed to the reversible formation of polymeric species at 0.8 V and the dissolution above 2.1 V in alkyl carbonate solution due to the high catalytic activity of the metal oxides nanoparticles.[27,28] The Coulombic efficiency of porous C/Sn anodes increased quickly from an initial 75% to almost 100% after 8 cycles. The porous C/Sn synthesized using simple carbonization technology showed a higher capacity and a longer cycling life than those C/Sn anodes reported in the literature.

To investigate the mechanism of the extra capacity in the porous C/Sn anode, the charge/discharge behaviors at different cycles were examined. Fig. 5c shows the charge/discharge behavior of the mesoporous Sn/carbon composite anodes in the 1st, 30th, 60th, 100th, and 150th cycles. Since the lithiation curves of the mesoporous C/Sn were interfered with by SEI formation during the initial few cycles, the delithiation curves were examined for the mechanism of the extra capacity. The first

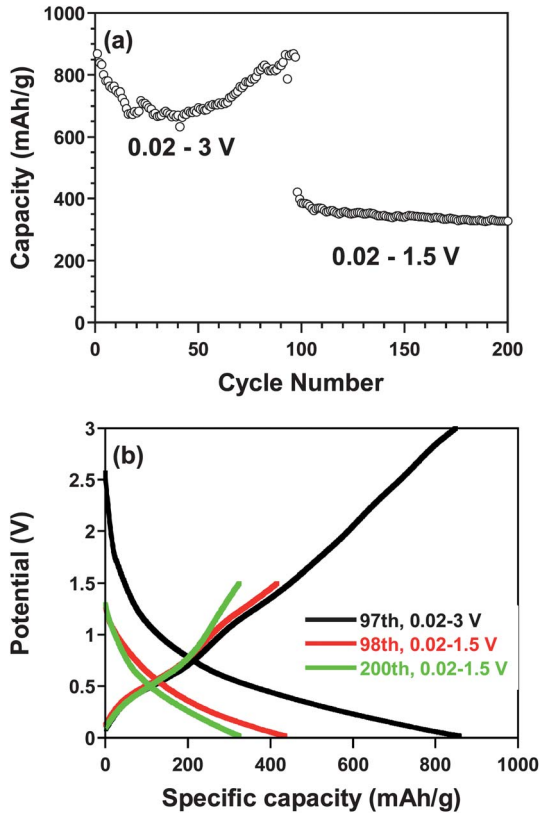

Fig. 6 (a) Cycling performance of the porous C/Sn composite cycled at 0.02–3 V and 0.02–1.5 V. (b) Charge/discharge curves at 0.02–3 V and 0.02–1.5V.

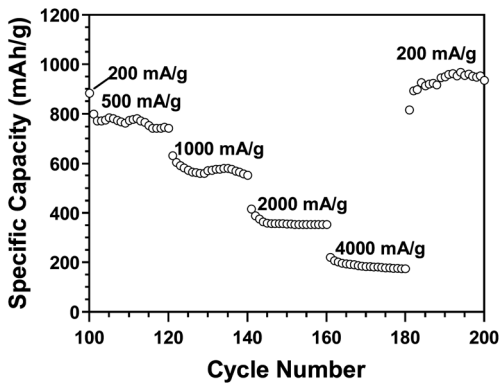

Fig. 7 Rate capability of the porous C/Sn composite at different current densities and 0.02–3 V after 100 cycles at 200 mA g^{-1}.

delithiation curve consists of three small plateaus at a potential around 0.6–0.8 V due to the formation of Li_xSn alloys, followed by a sloped line due to the lithiation of porous carbon. The decrease in delithiation capacity in the initial 30 cycles is mainly attributed to the reduced capacity of Li_xSn at a plateau potential of 0.8 V, as evidenced by the parallel delithiation curves of the first and the 30th cycles above 0.8 V. During further cycles, the capacity of the Li_xSn alloy was stable. However, the capacity above 1.2 V gradually increased. Here, we attributed the increased capacity above 1.2 V to the reversible decomposition of the gel-like polymer. The morphology of the gel-like polymer on the porous C/Sn anodes before decomposition was investigated using TEM after charging the electrode to 1 V (Fig. 5d). A thick layer of gel-like polymer was clearly observed on the surface of the composite anode. The extra capacity over the theoretical capacity due to the reversible formation of the polymeric species at 0.8 V and its dissolution above 2.1 V in alkyl carbonate solution was also found in metal oxide anodes (such as CoO,[27,28] CuO,[29] and SnO_2[23]). The decomposition potential (1.2 V) of the gel-like polymer on the porous C/Sn anode is much lower than that reported on CoO anodes (1.8 V).[27,28] This suggests that Sn has a higher catalytic activity for the reversible formation/decomposition of a gel-like polymer than the transition metals. The high catalytic role of Sn was also evidenced by the faster capacity increase in the mesoporous C/Sn than in the pure porous C anodes (Fig. 5b). It should be pointed out that the capacity delivered by the gel-like polymer on transition metal oxides anodes suffered a fast capacity fading after 100 cycles,[27,28] while the cycling stability of the mesoporous C/Sn composite was significantly improved, which was stabilized at 1300 mAh g^{-1} after 300 cycles.

If the delithiation capacity of the porous C/Sn anodes at a potential above 1.2 V is attributed to the decomposition of the gel-like polymer, the lithiation capacity due to formation of the gel-like polymer in the following discharge should decrease when the charge cut-off potential decreases from 3 V to 1.5 V. To confirm this hypothesis, a porous C/Sn anode was firstly cycled at 200 mA g^{-1} between 0.02 V and 3 V for 97 cycles, and was then charged/discharged at the same current but in a narrower potential range between 0.02 V and 1.5 V for an additional 103 cycles. Fig. 6a shows the capacity behavior of the porous C/Sn anodes in the total 200 charge/discharge cycles. The capacity retention during the charge/discharge cycles is showed in Fig. 6a, and the corresponding charge/discharge curves using different cut-off potentials at the 97th, 98th and 200th cycles were compared in Fig. 6b. As expected, the discharge capacity sharply decreased from 1040 mAh g^{-1} at the 97th cycle to ~420 mAh g^{-1} at the 98th cycle when the charge cut-off potential decreased from 3 V to 1.5 V (Fig. 6a). The capacity of the porous C/Sn anodes should continually increase if the charge cut-off potential is still maintained at 3 V (Fig. 5b), but abruptly declined when the charge cut-off potential was decreased to 1.5 V. This is because the formed gel-like polymer in the 97th discharge could not be decomposed at a potential below 1.5 V in the 98th charge, so no new gel-like polymer could be formed in the following discharge, resulting in a decrease of the discharge capacity at the 98th cycle. Therefore, the reduced species could not be fully oxidized at a potential below 1.5 V, leading to the extra capacity gradually vanishing (Fig. 6b). The exact mechanism behind the extra capacity for the mesoporous C/Sn anodes is still under investigation.

After the mesoporous Sn/carbon anodes were stabilized by charging/discharging for 100 cycles at 200 mA g^{-1}, the rate capability of the porous C/Sn composite was investigated at different currents. The excellent rate performance of the porous C/Sn anodes was demonstrated in Fig. 7. A high capacity of 360 mAh g^{-1} was retained at a current density of 2000 mA g^{-1}, which is much higher than the reported rate performance of C/Sn composite anodes using the electrostatic spray deposition (ESD) technique.[30] Even at a higher current of 4000 mA g^{-1}, the

capacity retention is still as high as 180 mAh g^{-1}. The enhanced rate capability is believed to be associated with the unique porous structure. The thin resilient carbon walls provide a mechanical support to enable good electric contact between tin particles and the carbon matrix. In addition, the large specific surface area ensures a high electrode–electrolyte contact area, which could significantly improve the transport for electrons and lithium ions.

Conclusions

A sponge-like porous carbon/tin nanoparticle composite was synthesized by simply dispersing SnO_2 nanoparticles in a polymer matrix and subsequent carbonization, where the self-assembled soft-template polymer decomposed during carbonization to form a porous structure. The porous Sn/C anodes can be charge/discharged for 450 cycles and maintain a reversible capacity of 1300 mAh g^{-1}, which is much higher than the theoretical capacity of the mesoporous C/Sn composite. The extra capacity is attributed to the high catalytic activity of Sn for the reversible formation/decomposition of a gel-like polymer. The C/Sn anodes with a unique porous structure can also deliver 360 mAh g^{-1} capacity even at 2000 mA g^{-1} charge/discharge current. In addition, the good thermal stability and simple synthesis make it very attractive as an anode for lithium ion batteries, especially for commercial manufacture.

Acknowledgements

The authors gratefully acknowledge the support of the Army Research Office under Contract No.: W911NF1110231 (Dr Robert Mantz, Program Manager) and Ellen Williams Distinguished Postdoctoral Fellowship.

References

1 U. Kasavajjula, C. S. Wang and A. J. Appleby, *J. Power Sources*, 2007, **163**, 1003.
2 J. W. Fergus, *J. Power Sources*, 2010, **195**, 939.
3 L. W. Ji, Z. Lin, M. Alcoutlabi and X. W. Zhang, *Energy Environ. Sci.*, 2011, **4**, 2682.
4 Y. G. Guo, J. S. Hu and L. J. Wan, *Adv. Mater.*, 2008, **20**, 2878.
5 P. G. Bruce, B. Scrosati and J. M. Tarascon, *Angew. Chem., Int. Ed.*, 2008, **47**, 2930.
6 V. L. Chevrier and G. Ceder, *J. Electrochem. Soc.*, 2011, **158**, A1011.
7 X. W. Lou, Y. Wang, C. L. Yuan, J. Y. Lee and L. A. Archer, *Adv. Mater.*, 2006, **18**, 2325.
8 Y. Wang, H. C. Zeng and J. Y. Lee, *Adv. Mater.*, 2006, **18**, 645.
9 G. Derrien, J. Hassoun, S. Panero and B. Scrosati, *Adv. Mater.*, 2007, **19**, 2336.
10 Y. Yu, L. Gu, C. B. Zhu, P. A. van Aken and J. Maier, *J. Am. Chem. Soc.*, 2009, **131**, 15984.
11 Y. Yu, L. Gu, C. L. Wang, A. Dhanabalan, P. A. van Aken and J. Maier, *Angew. Chem., Int. Ed.*, 2009, **48**, 6485.
12 I. S. Kim, G. E. Blomgren and P. N. Kumta, *Electrochem. Solid-State Lett.*, 2004, **7**, A44.
13 W. M. Zhang, J. S. Hu, Y. G. Guo, S. F. Zheng, L. S. Zhong, W. G. Song and L. J. Wan, *Adv. Mater.*, 2008, **20**, 1160.
14 K. T. Lee, Y. S. Jung and S. M. Oh, *J. Am. Chem. Soc.*, 2003, **125**, 5652.
15 Y. S. Jung, K. T. Lee, J. H. Ryu, D. Im and S. M. Oh, *J. Electrochem. Soc.*, 2005, **152**, A1452.
16 Y. Meng, D. Gu, F. Zhang, Y. Shi, H. Yang, Z. Li, C. Yu, B. Tu and D. Y. Zhao, *Angew. Chem., Int. Ed.*, 2005, **44**, 7053.
17 S. Tanaka, N. Nishiyama, Y. Egashira and K. Ueyama, *Chem. Commun.*, 2005, 2125.
18 C. Liang and S. Dai, *J. Am. Chem. Soc.*, 2006, **128**, 5316.
19 J. C. Guo, X. L. Chen and C. S. Wang, *J. Mater. Chem.*, 2010, **20**, 5035.
20 J. C. Guo, A. Sun and C. S. Wang, *Electrochem. Commun.*, 2010, **12**, 981.
21 J. Hassoun, G. Derrien, S. Panero and B. Scrosati, *Adv. Mater.*, 2008, **20**, 3169.
22 D. Deng and J. Y. Lee, *Angew. Chem., Int. Ed.*, 2009, **48**, 1660.
23 B. Guo, J. Shu, K. Tang, Y. Bai, Z. Wang and L. Chen, *J. Power Sources*, 2008, **177**, 205.
24 S. Yang, X. Feng, L. Zhi, Q. Cao, J. Maier and K. Müllen, *Adv. Mater.*, 2010, **22**, 838.
25 P. Lian, X. Zhu, S. Liang, Z. Li, W. Yang and H. Wang, *Electrochim. Acta*, 2011, **56**, 4532.
26 A. Magasinski, P. Dixon, B. Hertzberg, A. Kvit, J. Ayala and G. Yushin, *Nat. Mater.*, 2010, **9**, 353.
27 S. Laruelle, S. Grugeon, P. Poizot, M. Dollé, L. Dupont and J.-M. Tarasconz, *J. Electrochem. Soc.*, 2002, **149**, A627.
28 S. Grugeon, S. Laruelle, L. Dupont and J.-M. Tarascon, *Solid State Sci.*, 2003, **5**, 895.
29 A. Débart, L. Dupont, P. Poizot, J.-B. Leriche and J. M. Tarascon, *J. Electrochem. Soc.*, 2001, **148**, A1266.
30 X. Li, A. Dhanabalan and C. Wang, *Adv. Energ. Mater.*, 2012, **2**, 238.

